Dynamic Load Measurements with Delta Wings Undergoing Self-Induced Roll Oscillations

Daniel Levin* and Joseph Katz†
Technion, Israel Institute of Technology, Haifa, Israel

The aerodynamic forces acting on a delta wing mounted on a free-to-roll sting-balance apparatus were measured. Two wing planforms having leading edge sweeps of 76 and 80 deg were tested, however, only the wing with the 80 deg sweep would undergo periodic self-induced roll oscillations. The time dependent forces and roll angles for this wing were then recorded for various test conditions. In these tests a considerable drop in the average normal force of the free-to-roll wing was measured, relative to the normal force obtained in the static tests. Also, the helium-bubble flow visualization technique was used to gain some insight into the periodic motion of the separated leading-edge vortices.

Nomenclature

$\mathcal{R}$ = wing aspect ratio
b = wing span
c = wing chord
C_{NOR} = normal force coefficient (in balance coordinates)
C_{ROLL} = rolling moment coefficient (in balance coordinates), $C_{ROLL} = \dfrac{\text{Rolling Moment}}{\frac{1}{2}\rho V^2 Sb}$
C_Y = side force coefficient (in balance coordinates)
S = wing area
V = wind tunnel air speed
α = angle of attack
β = side slip angle
ρ = air density
ϕ = roll angle
ω = frequency of roll oscillations
$(\ )_0$ = initial condition

Introduction

Self-induced roll oscillations are major limitation on the low speed maneuvers of aircraft utilizing highly swept wing planforms. At flight conditions, such as short landing at high angle of attack on carriers, these oscillations commonly known as "wing rock" can present a safety problem that must be accounted for when designing the aircraft control mechanism. Such mechanisms can be established on the basis of a simplified mathematical model[1-6] that will describe this highly nonlinear aerodynamic phenomenon. The aerodynamic coefficients for this model, however, must be obtained by a detailed measurement of the acting forces, frequencies, and their phase relation. On the other hand, due to time dependency of the dynamic quantities in such experiments these measurements are rather complex and the reported data in the literature is minimal.

Recently, Nguyen et al.[7] successfully recorded roll angle oscillations during self-induced wing rock of a flat plate delta wing with 80 deg leading edge sweep, and then calculated the resulting rolling moments. The rolling axis of their free to roll model was mounted, however, under the wing planform, resulting in a partial coning motion in addition to the pure roll oscillations.

The present work is a continuation of these reported efforts to gain some experimental insight into the self-induced wing rock phenomenon. In addition to the roll angle measurement, normal and side forces and their phase relation were measured. The models were mounted on a sting-balance apparatus and were free to oscillate about their geometrical axes, resulting in a pure roll oscillation.

Experimental Apparatus

The delta wing models were mounted on the sting-balance as shown in Fig. 1. The cross section of the wind tunnel was 1m × 1m and maximal airspeed was 32 m/sec (corresponds to $Re = 0.5 \times 10^6$ based on wing No. 1 chord). The two wing planforms, shown in Figure 2, were fabricated so that their rolling axis coincided with both balance and wing geometrical axes. Phase angle was recorded by a rotary potentiometer located ahead of the front bearing, whereas the sting-balance mounting was capable of transmitting three force and three moment components from the model. The electrical signal from the balance could be digitally reduced or analogically plotted versus time, both on a mechanical and on an optical recorder.

Results

The testing of the models shown in Fig. 2 were conducted in two regimes, the static testing regime and the dynamic regime. The static test results covered a wide range of angle of attack, angle of side slip, and roll angles. Based on this data, nonlinearities in the rolling moment slope were detected. The dynamic experiments consisted of mounting the wings on a free-to-roll balance and then measuring normal and side forces and rolling angles. Vortex patterns in the unsteady flow were traced by helium-bubble flow-visualization, providing dynamic information about the vortex wake motion, which plays an important role during the "wing rock" cycle.

Static Tests

The results of the static tests for both wings are summarized in Fig. 3a-8b. The normal force variation C_{NOR} (in balance coordinates) vs angle of attack α is shown in Fig. 3a for various side slip angles β. For the $\beta = 0$ condition, wing stall occurs above 40 deg, which is slightly higher than those reported in the literature.[7] As the yaw angle is increased, the normal force "first stall" regresses to a smaller angle of

Received Aug. 17, 1982; revision received July 20, 1983.

*Faculty of Aeronautical Engineering. Member AIAA.
†Faculty of Mechanical Engineering. Member AIAA.

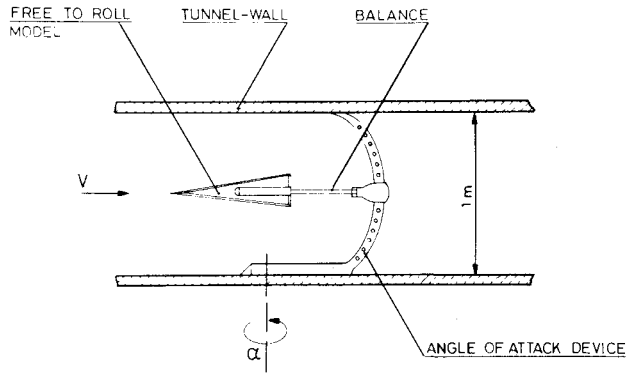

Fig. 1 The delta wing model as mounted in the wind-tunnel test section.

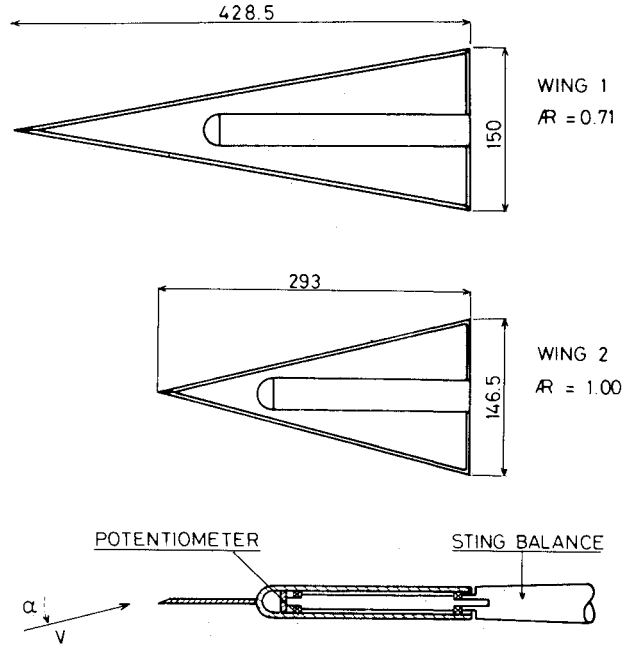

Fig. 2 Free-to-roll delta wing models.

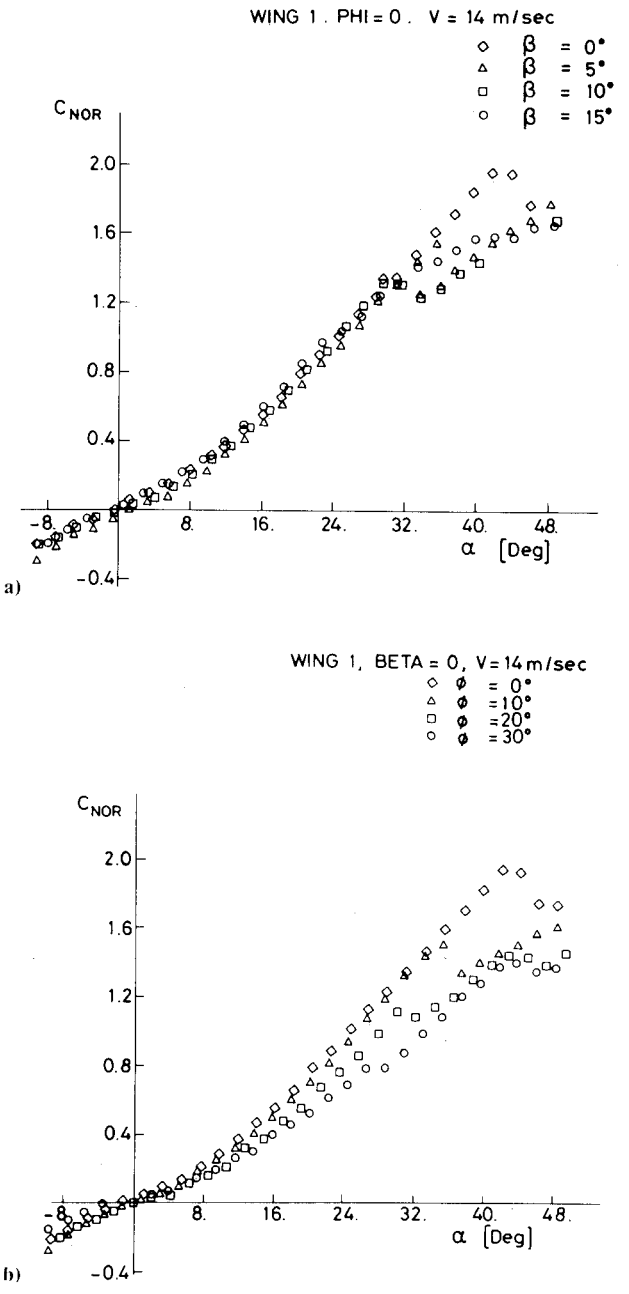

Fig. 3 Variation of normal force coefficient vs angle of attack (wing 1).

attack (down to $\alpha = 24$ deg at $\beta = 15$ deg). Similar behavior is observed when the roll angle ϕ is varied instead of the side-slip angle β (Fig. 3b). The reduction in C_{NOR} for this case is a result of multiplication by $\cos\phi$, since the balance records only the vertical component.

When the wing rolling moment C_{ROLL} is considered (Fig. 4a), a similar behavior is observed, that is, the normal force stall results in a "rolling moment stall" at the same angle of attack. The curve of $\beta = 5$ deg in Fig. 4a is similar in nature to the usual $\partial C_{ROLL}/\partial\beta$ curve, and for angles of attack under stall an almost linear derivative is observed. Beyond $\alpha = 35$ deg, however, a change in sign of $\partial C_{ROLL}/\partial\beta$ is measured, which results in a destabilizing effect.

The rolling moment vs roll angle ϕ is shown in Fig. 4b and it is basically similar to the data presented in Fig. 4a since the angle ϕ can always be divided into components of angle of attack α and side-slip β. In addition to Fig. 4, a crossplot of the data is presented in Fig. 5. The rolling moments obtained are slightly higher than those reported by Shanks[8], which is probably a result of the central mounting of the wings, as shown in Fig. 2. Because of this mounting, the central cylinder (Fig. 2) slightly dislocated the separated vortex cores to the outward direction and in the presence of side slip this caused the higher C_{ROLL} values.

The static characteristics of Wing 2 are summarized in the normal force plots of Fig. 6, the rolling moment plots of Fig. 7, and the crossplots of Fig. 8. There is no major difference between the data of Wing 1 and Wing 2. Thus, an explanation of why the first wing exhibited self-induced roll oscillations and the other did not cannot be based solely on the static data.

Dynamic Tests

In these experiments the two delta wings were mounted on a free-to-roll balance. Wing 1 exhibited self-induced roll oscillations while Wing 2 did not. This was the case even when, under various angles of attack, roll oscillations were forced up to $\phi_{max} = 40$ deg on Wing 2. It is concluded, therefore, that in order to maintain steady roll oscillations under similar conditions (e.g. Re number, bearing friction and wing moment of inertia), the wing aspect ratio probably must be smaller than 1.

The development of "wing rock" condition in the free-to-roll model is shown in Fig. 9. The increase in the normal force at the first interval is due to wind-tunnel airspeed acceleration. At the second interval the normal force is stabilized while recorded roll angle is still $\phi = 0$. The third

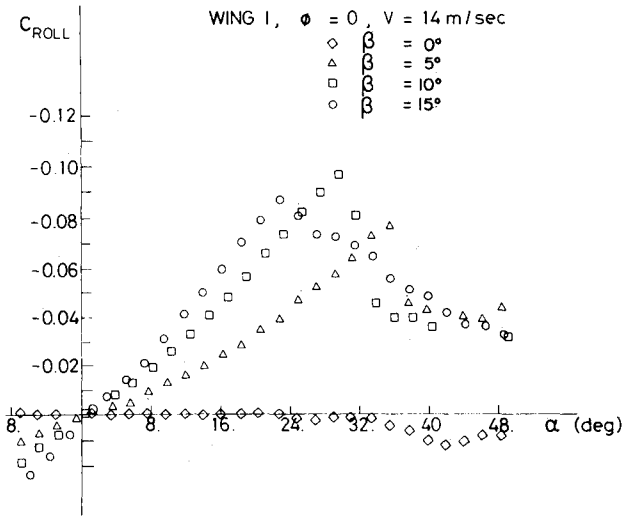

a) Effect of side slip β

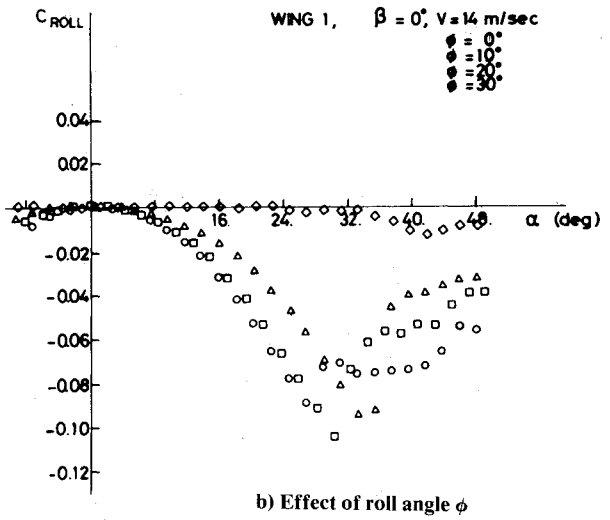

b) Effect of roll angle ϕ

Fig. 4 Rolling moment vs angle of attack (wing 1).

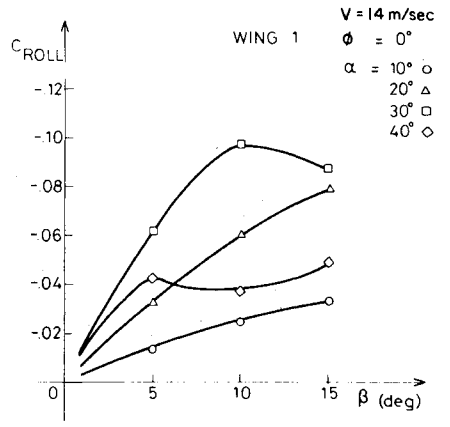

Fig. 5a Rolling moment vs side slip (wing 1).

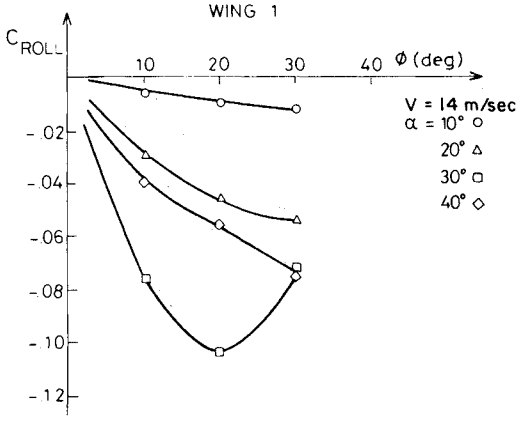

Fig. 5b Rolling moment vs roll angle (wing 1).

interval starts after a random disturbance has initiated the rolling process and then a steady periodic oscillatory condition develops. As a result of these oscillations, normal force loss occurs—a phenomenon that might be hazardous to a real aircraft entering similar conditions.

The timewise variation of side force and normal force, as measured in the balance coordinates and also the roll angle ϕ, is shown in Figs. 10-13 for $\alpha = 20$ deg, 25 deg, 30 deg, and 35 deg, respectively. Side force oscillations are in phase with roll angle ϕ and have the same frequency, whereas the normal force oscillates with double frequency[7]. Also, side force amplitude is much larger than normal force amplitude and this will have a strong effect on a free flight model. Figs. 10-13 indicate, too, that a phase lag in C_Y, relative to the phase angle ϕ, is present. This phase lag will grow moderately from $\alpha = 20$ deg (Fig. 10) up to several degrees at $\alpha = 35$ deg (Fig. 13). Accurate measurements of this phase lag, however, were not attainable by the current experimental setup. For smaller angles of attack (19.5 deg $< \alpha < 25$ deg), the wind-tunnel "natural disturbance" was too low to initiate self-induced roll oscillations. For this range, therefore, the oscillations were obtained at a higher angle of attack, which was then reduced. By this method stable periodic oscillations were present down to $\alpha = 19.5$ deg.

At the upper boundary of angle of attack this problem did not exist. In this range of 51 deg $> \alpha > 50$ deg, the oscillations were steady but roll angle amplitudes were fluctuating, whereas at $\alpha = 51$ deg the oscillations ceased, independently of the direction that the angle of attack was approached at. Above $\alpha = 51$ deg wind tunnel disturbance eventually introduced some rolling motion which was then rapidly damped. Consistency was checked by repeating the same experiment for different starting conditions (α or β), but the values for both force data and rolling angles ϕ returned to their initial value.

When comparing the normal force obtained in the dynamic test to the static test results, it is found that the average dynamic value $C_{NOR\,|\,dynamic}$ is less than the projection of $C_{NOR\,|\,static}$ by some average roll angle ϕ_{av} ($\phi_{av} \cong \phi_{max}/2$):

$$C_{NOR\,|\,dynamic} < C_{NOR|\,static} \times \cos\phi_{av} \tag{1}$$

On the other hand, from Fig. 9-13 it is found that:

$$C_{Y_{max}\,|\,dynamic} \geq C_{NOR\,|\,static} \times \sin\phi_{max} \tag{2}$$

These quantities of equation (1) and (2) would be expected to be equal if wing normal force would stay constant, and the dynamic side force and normal force would be the result of their projection due to the angle ϕ.

As an example the results of Fig. 10 and Fig. 12 can be compared with the static data of Fig. 3b. For $\alpha = 20$ deg the maximal recorded roll angle was on the order of $\phi_{max} \sim 14$ deg (Fig. 10) and the average normal force $C_{NOR} \sim 0.64$. This value is far less than the values obtained by the static tests ($C_{NOR} = 0.8$ for $\phi = 0$ deg and $C_{NOR} = 0.65$ for $\phi = 15$ deg),

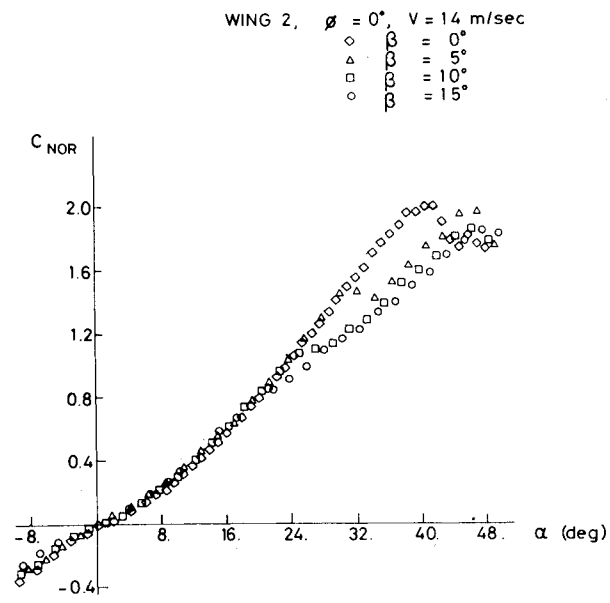

a) Effect of side slip β

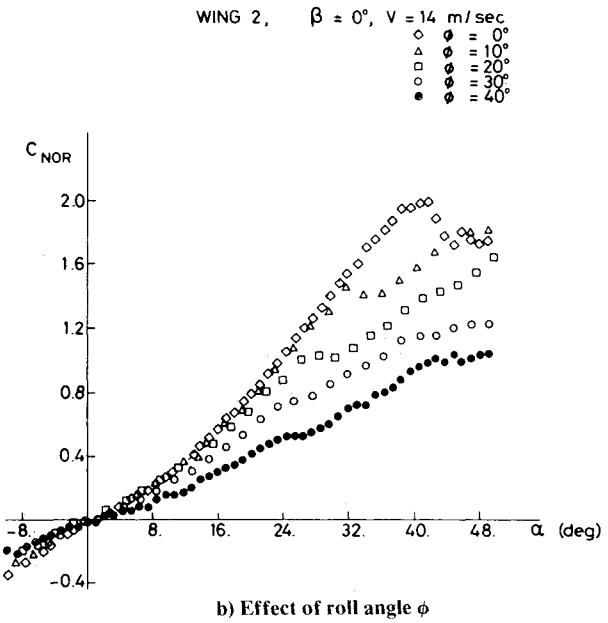

b) Effect of roll angle ϕ

Fig. 6 Variation of normal force coefficient vs angle of attack (wing 2).

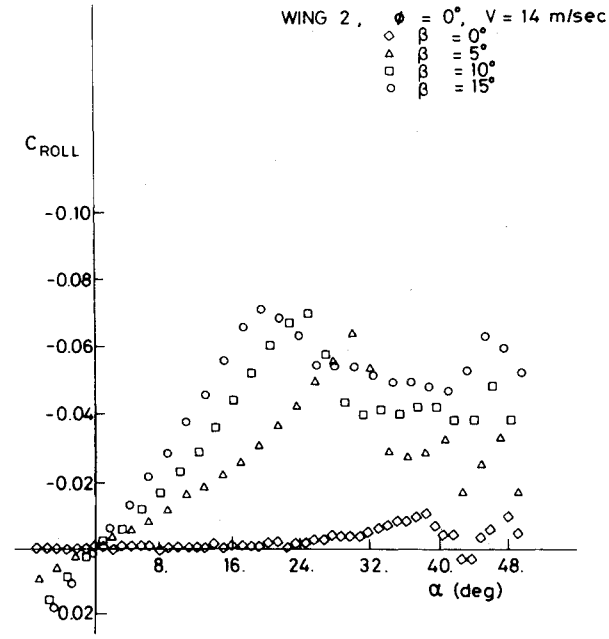

a) Effect of side slip β

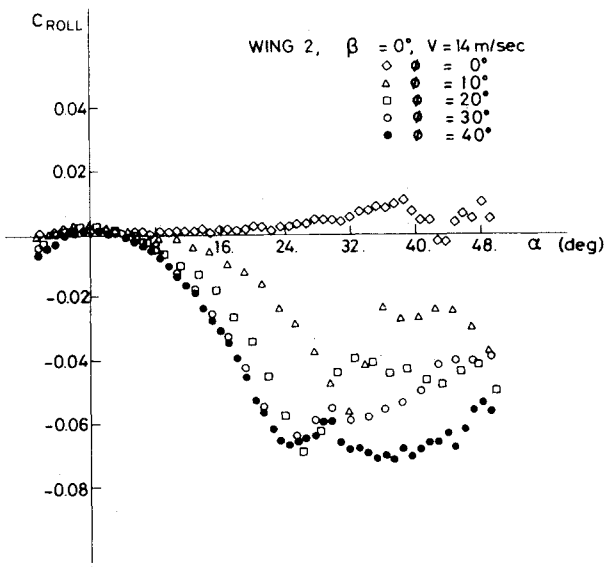

b) Effect of roll angle ϕ

Fig. 7 Rolling moment vs angle of attack (wing 2).

which would call for a normal force oscillation in the range of $C_{NOR} = 0.8$-0.65. A similar trend is observed in Fig. 12, where the maximal dynamic roll angle was $\phi_{max} = 28$ deg for $\alpha = 30$ deg. The normal force variation according to Fig. 3b should then be between $C_{NOR} = 1.28$ (for $\phi = 0$) and $C_{NOR} = 0.8$ (for $\phi = 30$ deg). However, the average dynamic normal force in Fig. 12 is $C_{NOR} \sim 0.65$ which is far less than the range which would be expected based on the static data. It is concluded therefore that the forces acting in the dynamic condition are more complex and that an extrapolation based on static data might be misleading.

Sample results of the flow visualization experiments by the helium-bubble technique are presented in Fig. 14. Since lighting conditions were minimal the dynamic visualization was recorded first on a video-tape and some frames were then photographed. It was observed that vortex breakdown position oscillates with wing roll oscillations, that is, when one side of the wing rolls down, then the breakdown of that side will advance forward. Also, at $\alpha = 22$ deg the vortex breakdown pattern approaches the trailing edge, whereas under static condition it would have stayed far behind the trailing edge[9] (This is probably due to the additional upwash induced by the wing downward-rolling motion.) When angle of attack is increased to $\alpha = 25$ deg and $\alpha = 32$ deg, the breakdown pattern can clearly be seen over the wing upper surface. In these cases, too, the vortex breakdown position is found to be forward to its static location.

The range of angle of attack α at which roll oscillation will take place is plotted in Fig. 15. At an angle of attack $\alpha = 19$-20 deg, the self induced roll oscillation will begin for wing 1 and will be present up to $\alpha = 50$-51 deg. Maximal roll angles will be larger for the smaller angles of attack, whereas their magnitude will decrease up to $\alpha = 51$ deg. The reduced frequency $\omega c/V$ increases moderately with increasing angle of attack,up to the point where the oscillations will cease ($\alpha = 51$ deg).

The effect of increasing the wind-tunnel speed is to increase the roll angle amplitude (as shown in Fig. 16), whereas the

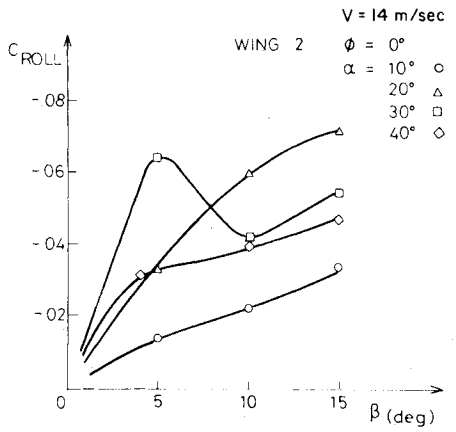

Fig. 8a Rolling moment vs side slip (wing 2).

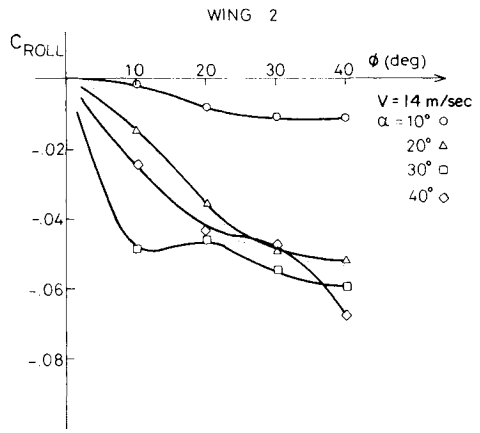

Fig. 8b Rolling moment vs roll angle angle (wing 2).

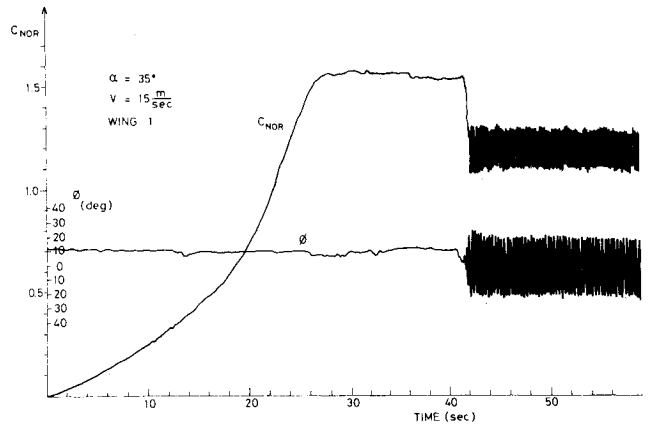

Fig. 9 Development of "wing rock."

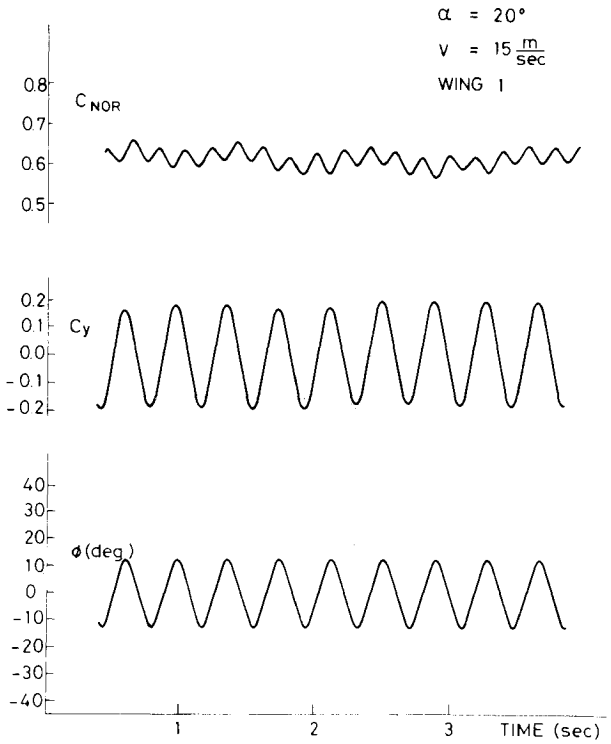

Fig. 10 Time history of "wing rock," $\alpha = 20$ deg

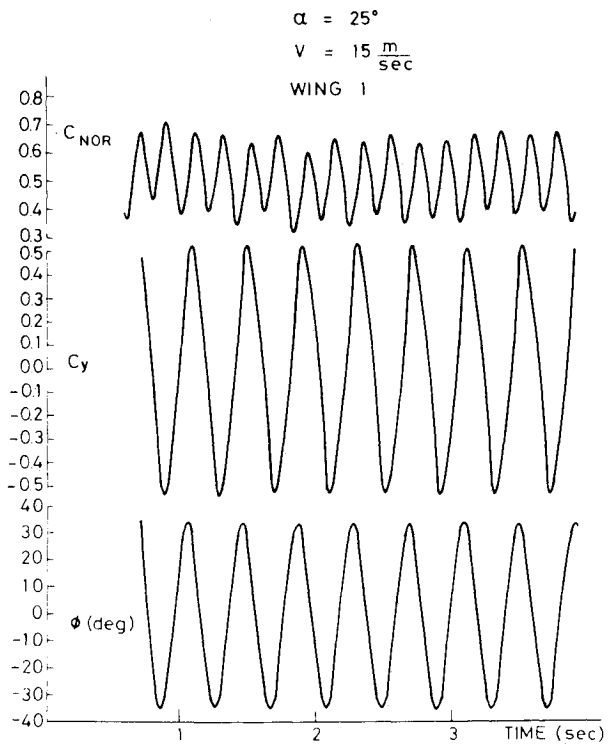

Fig. 11 Time history of "wing rock," $\alpha = 25$ deg.

reduced frequency stays almost unchanged. The range of the initial wing positions in the wind tunnel, that led to the development of self-induced roll oscillations in the present experiment, is presented in Fig. 17. Since the wing was mounted on a free-to-roll axis, the only condition for "wing rock" was that the equivalent windward angle of attack be more than 19.5 deg and less than 51 deg or:

$$tg^2 19.5 \text{ deg} < tg^2\alpha_0 + tg^2\beta_0 < tg^2 51 \text{ deg} \qquad (3)$$

where α_0 and β_0 are the initial angle of attack and side slip, respectively, measured relative to freestream velocity V. All the peripheral points within the "self-induced roll oscillations" region of Fig. 17 were actually measured. For example, if the wing was initially positioned at $\alpha = 0$ deg and $\beta = 19.5$ deg or $\beta = 51$ deg, the motion would be started by the initial rolling moment, caused by the wing leading-edge slant (Fig. 2).

Concluding Remarks

In the present work both static and free-to-roll dynamic tests were conducted with two flat plate delta wings. It was

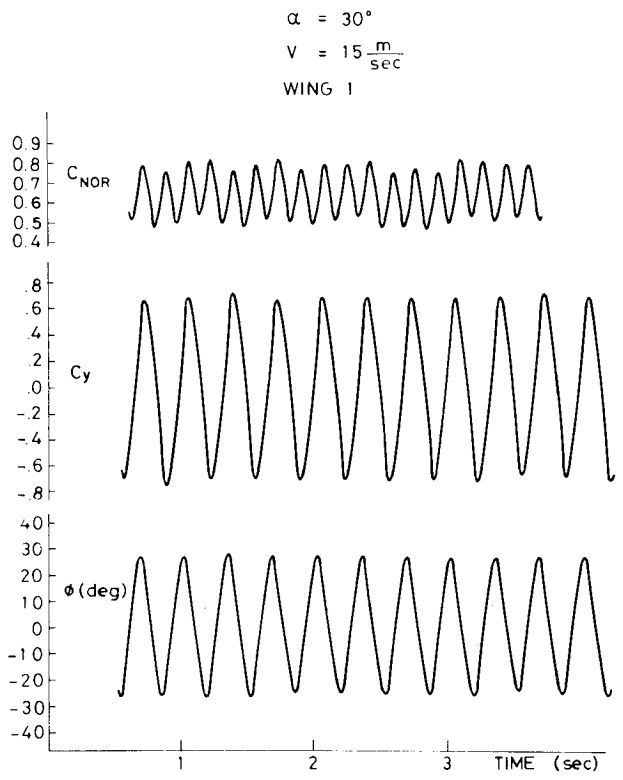

Fig. 12 Time history of "wing rock," $\alpha = 30$ deg

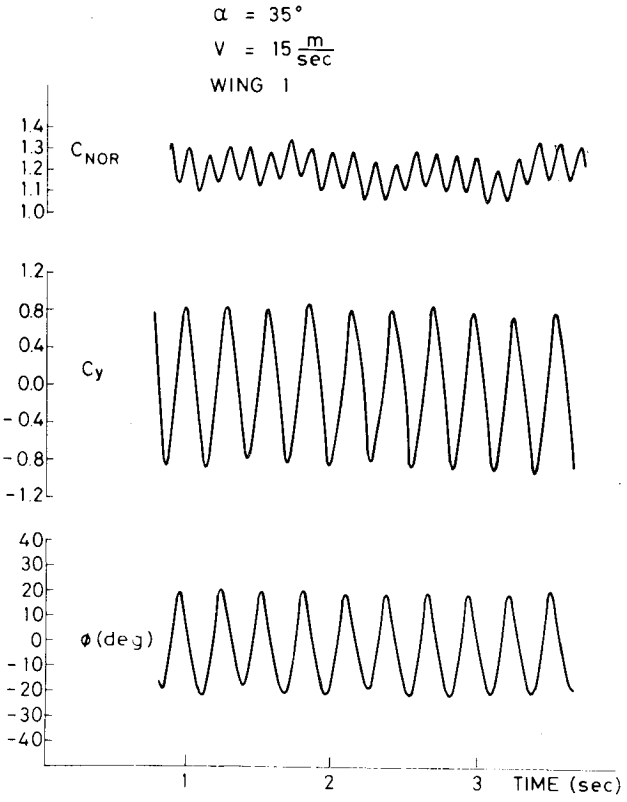

Fig. 13 Time history of "wing rock," $\alpha = 35$ deg.

found that the narrower wing with the aspect ratio of 0.71 exhibited self-induced roll oscillations while the wing with the aspect ratio of unity, having the higher damping in roll coefficient, did not exhibit such motion. During the free-to-roll tests a loss in wing average lift was detected, relative to the static lift for the same angle of attack. Also, the oscillation

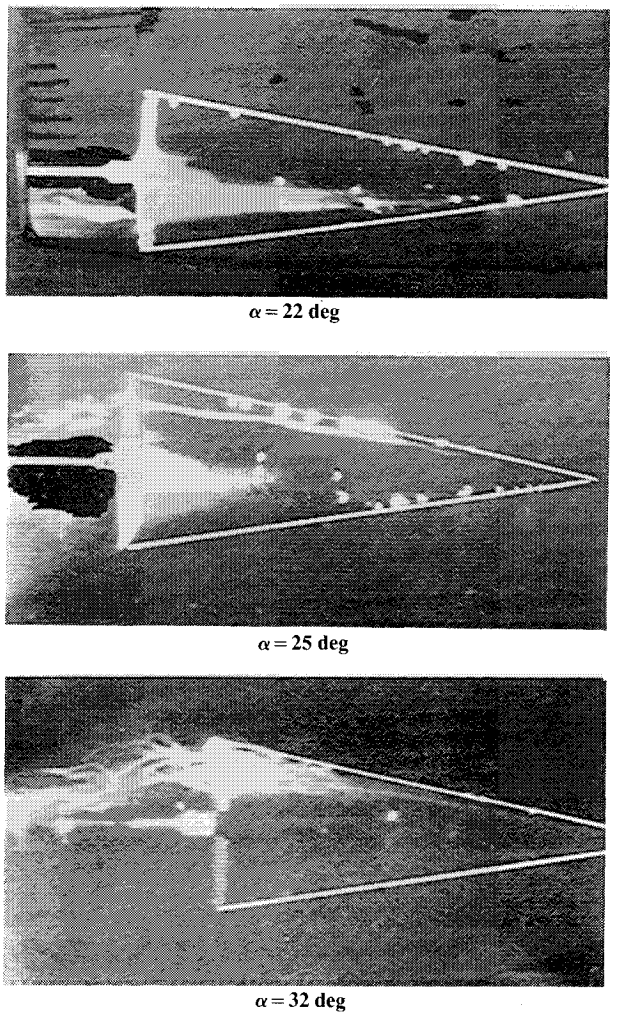

$\alpha = 22$ deg

$\alpha = 25$ deg

$\alpha = 32$ deg

Fig. 14 Dynamic vortex bursting position during wing rock (most forward position during the cycle).

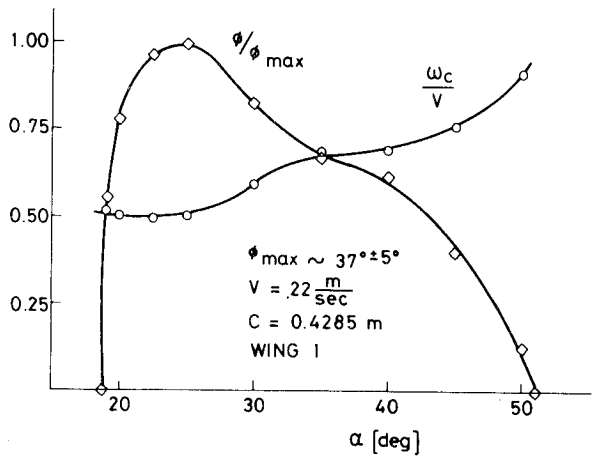

Fig. 15 Variation of roll angle amplitude and frequency vs angle of attack.

frequencies and their variations with wind tunnel speed and angle of attack were recorded, along with side force and normal force amplitudes.

The two major questions in regard to this phenomena are: 1.) What is the mechanism leading to the self induced oscillations? and 2.) What is the reason for the reduction in the average normal force? A possible explanation, based on the data presented is that these oscillations are sustained due

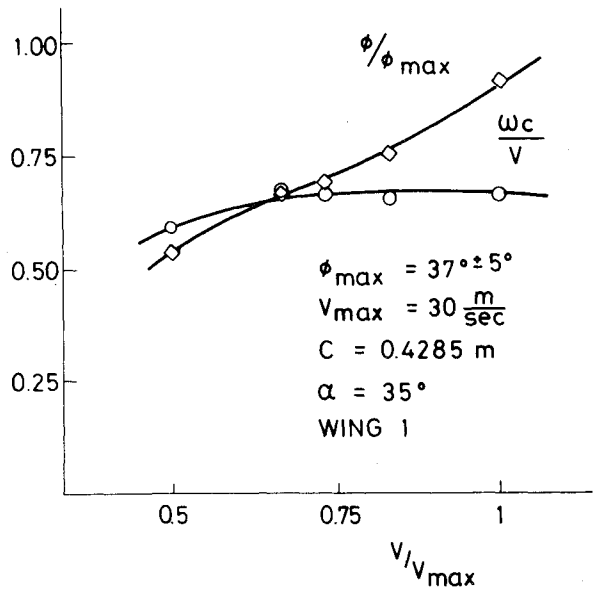

Fig. 16 Variation of roll angle amplitude and frequency vs wind-tunnel air-speed.

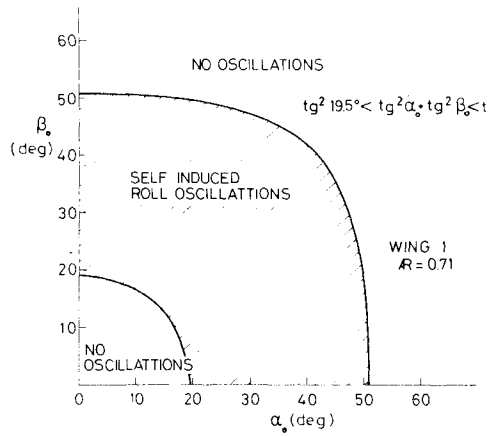

Fig. 17 The range of initial wing positions ($\alpha_0 \beta_0$) from which self-induced roll oscillations can develop.

to the momentarily reduced distance between the up-moving semi-wing and leading-edge vortex originating from the same side. Thus, during the upward motion of this particular wing section a higher vortex suction force will be present, resulting in a dynamic rolling moment, which is larger than the static value. This effect is also the reason for the phase lag in the side force C_Y, shown by Fig. 10-13. On the other hand, vortex breakdown, as presented in Fig. 14, must have a damping effect on this motion, since flow visualizations indicated that the vortex burst is delayed relatively to the occurrence of maximal roll angle. Furthermore, since under dynamic conditions the wing upper surface is exposed to a more forward vortex breakdown, the average lift becomes less than the static value. In addition, during most of the roll cycle, only one leading-edge vortex is present above the wing, whereas at zero roll condition two of these vortices are present. Therefore, the reduction in the magnitude of the vortex lift, under the dynamic conditions, is obvious.

In conclusion, the "wing rock" condition can develop when the work done during the roll cycle, by destabilizing vortex interactions (due to reduced distance between the up-moving semi-span and the leading edge-vortex), overcomes the energy dissipation of the wing damping forces. When this damping is increased as a result of higher aspect ratio or higher angle of attack (and vortex burst-damping), however, the oscillations will be terminated.

Acknowledgements

The work presented herein was supported under NASA Grant No. NAGW-00218. Dr. Lewis B. Schiff acted as project monitor.

References

[1]Tobak, M. and Schiff, L. B., "A Nonlinear Aerodynamic Moment Formulation and Its Implications for Dynamic Stability Testing," AIAA Paper 71-275, March, 1971.

[2]Tobak, M. and Schiff, L. B., "Nonlinear Aerodynamics of Aircraft in High-Angle-of-Attack Maneuvers," AIAA Paper 74-85, Feb. 1974.

[3]Tobak, M. and Schiff, L. B., "On the Formulation of the Aerodynamic Characteristics in Aircraft Dynamics," NASA TR R-456, Jan. 1976.

[4]Tobak, M. and Schiff, L. B., "The Role of Time-History Effects in the Formulation of the Aerodynamics of Aircraft Dynamics." AGARD CP-235, Paper 26, May 1978.

[5]Schiff, L. B., Tobak, M., and Malcolm, G. N., "Mathematical Modelling of the Aerodynamics of High-Angle-of-Attack Maneuvers," AIAA Paper 80-1583, Aug. 1980.

[6]Schmidt, L. V., "Wing Rock Due to Aerodynamic Hysteresis," *Journal of Aircraft*, Vol. 16, March 1979.

[7]Nguyen, L. T., Yip, L., and Chambers, J. R., "Self-Induced Wing Rock of Slender Delta Wings." AIAA Paper 81-1883, Aug. 1981.

[8]Shanks, R. E., "Low Subsonic Measurements of Static and Dynamic Stability Derivatives of Six Flat-Plate Wings Having Leading Edge Sweep Angles of 70 deg to 84 deg," NASA TND-1822, July 1963.

[9]Polhamus, E. C., "Predictions of Vortex-Lift Characteristics by a Leading-Edge Suction Analogy," *Journal of Aircraft*, Vol. 8, 1971, pp. 193-199.